INVESTIGATION OF A SMALL HYDROGEN-OXYGEN ROCKET ENGINE

R. Sandri, et al

National Research Council of Canada
Ottawa, Ontario, Canada

August 1973

National Research Council Canada
Conseil national de recherches Canada

INVESTIGATION OF A SMALL HYDROGEN-OXYGEN ROCKET ENGINE

BY
R. SANDRI, R. BILLINGHAM AND F. CHELLINGWORTH
DIVISION OF MECHANICAL ENGINEERING

OTTAWA
AUGUST 1973

NRC NO. 13556

MECHANICAL ENGINEERING REPORT
MP-64

31

INVESTIGATION OF A SMALL HYDROGEN - OXYGEN ROCKET ENGINE

RECHERCHES SUR UN PETIT MOTEUR DE FUSEE A HYDROGEN ET OXYGENE

by/par

R. SANDRI, R. BILLINGHAM AND/ET F. CHELLINGWORTH

R. B. Whyte, Head/Chef
Fuels and Lubricants Laboratory/
Laboratoire des combustibles et lubrifiants

D. C. MacPhail
Director/Directeur

/

SUMMARY

An investigation on a small water-cooled, liquid oxygen/liquid hydrogen rocket engine has established the design of an efficient combustion system using a low pressure-drop injector. Five different injector combinations were considered and their combustion efficiencies evaluated. Heat transfer measurements were made and the effects of injector design on heat transfer profiles studied. Preliminary investigations were also made on a regeneratively-cooled combustion chamber, using hydrogen flowing through a simple annular cooling passage.

RESUME

On a effectué des recherches sur un petit moteur de fusée à oxygène liquide et hydrogène liquide avec refroidissement par eau qui ont permis d'aboutir à la conception d'un système de combustion efficace utilisant un injecteur à faible chute de pression. On a étudié cinq différentes combinaisons d'injecteurs et étudié leur rendement de combustion. On a également fait des mesures de transmission de chaleur et des études sur les effets de la conception de l'injecteur sur les profils de transmission de chaleur. Des recherches préliminaires ont aussi été effectuées sur une chambre de combustion refroidie en faisant circuler de l'hydrogène liquide dans un anneau.

TABLE OF CONTENTS

TABLES

ILLUSTRATIONS

ILLUSTRATIONS (Cont'd)

SYMBOLS

Symbol	Definition
A	reference area (cm^2)
A_c	combustion zone area (cm^2)
A_t	throat area (cm^2)
C^*	characteristic velocity (ft/sec)
C^*_A	measured characteristic velocity (ft/sec)
C^*_c	corrected theoretical characteristic velocity (ft/sec)
D	hydraulic mean diameter (cm)
D_1	chamber casing inside diameter (cm)
D_2	chamber liner outside diameter (cm)

SYMBOLS (Cont'd)

Symbol	Definition
D_t	throat diameter (cm)
g	gravitational acceleration (ft/sec^2)
ΔH_c	heat gain of water coolant (CHU/sec)
ΔH_{ch}	coolant heat gain of hydrogen (CHU/sec)
ΔH_h	heat gain of hydrogen (CHU/sec)
h_c	film coefficient of water coolant
h_g	film coefficient of combustion gases
k	thermal conductivity of chamber wall (cal/cm sec °C)
Mc	mach number of combustion gases
m	molecular weight of combustion gas products
p_i	static pressure at injector face (psia)
p_c	static pressure in combustion zone (psia)
p_h	hydrogen injector pressure-drop (psi)
p_o	stagnation pressure in combustion zone (psia)
p_{ox}	oxygen injector pressure-drop (psi)
q	heat transfer rate ($CHU/cm^2/sec$)
R	radius of curvature of throat nozzle contour (cm)
R_1	universal gas constant (2780 ft lb/mole °C)
T_c	combustion gas temperature (°K)
Tcc	corrected combustion gas temperature (°K)
Taw	adiabatic wall temperature of combustion gas (°K)
Tgi	hydrogen gas temperature (injector inlet) (°K)

SYMBOLS (Cont'd)

Symbol	Definition
T_{wg}	chamber wall temperature (combustion side) (°K)
T_{wc}	chamber wall temperature (coolant side) (°K)
T_{co}	coolant bulk temperature (°K)
t	chamber wall thickness (cm)
V_{co}	velocity of coolant (cms/sec)
$\bar{w}$	total propellant flow (lb/sec)
C_p	specific heat of combustion gas (cals/gram °K)
γ	ratio of specific heats of combustion gases
μ	viscosity of combustion gases (poises)
P_r	Prandtl number $= \frac{\mu C_p}{k}$

INVESTIGATION OF A SMALL HYDROGEN - OXYGEN ROCKET ENGINE

1.0 INTRODUCTION

This report describes experimental and theoretical investigations made on a small hydrogen-oxygen rocket engine. Such an engine could be used to power the last stage of a rocket vehicle capable of placing a moderate payload into near-earth orbit[1,2].

This work was a natural continuation of preliminary investigations made into small rocket systems[3,4]. The primary object was to establish a suitable design for an efficient low-pressure combustor and study its heat transfer characteristics. The work was conducted in two phases: first, using a water-cooled combustion chamber, and second, using a regeneratively-cooled chamber with hydrogen as the coolant.

WATER-COOLED COMBUSTION CHAMBER

2.0 GENERAL DESCRIPTION

The stainless steel water-cooled combustion chamber, shown in Figure 1, was designed to operate at a combustion pressure of 60 psia which expanded to an exhaust pressure of 9 psia. The design oxygen to fuel weight ratio was 4.76/1 and the nominal thrust at ambient pressure was 288 lb. The injector consisted of a central igniter chamber surrounded by four equally spaced swirl type oxygen injectors and a plain orifice combination through which the hydrogen was injected. To facilitate ease and economy of manufacture the injectors were made from brass with silver-soldered joints. The oxygen swirl injectors were made in stainless steel and screwed into the injector face. The design of this simple swirl atomizer was based on established gas turbine fuel system practice[5]. See Figure 2. Initial combustion was established in the igniter chamber using a hypergolic combination of chlorine trifluoride and hydrogen, which in turn ignited the main propellants. The water coolant entered the cooling jacket at the injector end to flow longitudinally through an annular passage of constant height (0.062 in) before exhausting to atmosphere through a large number of small holes. The approximate water flow was 10 lb/sec and entered the jacket at about 75 psig.

The complete system is shown schematically in Figure 3. All propellants were fed to the combustion chamber by pressurized gas; helium for the oxygen and hydrogen systems and nitrogen for the water and chlorine trifluoride systems. Though the oxygen and hydrogen systems drew their gas from a common source, each had its own pressurizing system and all precautions were taken to ensure no interaction between them.

The tank containing liquid oxygen was suspended inside a vacuum-jacketed Dewar which had a loose-fitting top. When the tank was filled with liquid oxygen it became effectively surrounded by an insulating blanket of very cold still air, as did a turbine flowmeter in the liquid oxygen feed line. The pressurizing and vent system was mounted on the Dewar top, the remaining control and feed valves were mounted close to the injector/combustion chamber.

The liquid hydrogen tank was suspended inside a vacuum-jacketed Dewar which had a sealed top. During operation both the tank and the Dewar contained liquid hydrogen, the Dewar hydrogen being at atmospheric pressure. The atmospheric liquid hydrogen served a double purpose. It stabilized the inner tank liquid temperature and the turbine flowmeter temperature, the latter being installed in the hydrogen feed line. It also was the source from which we filled the inner tank by means of an externally controlled fill valve. The pressurizing and vent system was again mounted on the Dewar top with the remaining control and feed valves mounted close to the injector/combustion chamber. To conserve liquid hydrogen, the helium pressurizing gas was passed through a cooling coil, immersed in a liquid nitrogen Dewar, before entering the liquid hydrogen tank. Liquid hydrogen leaving the tank was passed through a heat exchanger (liquid nitrogen) to convert it to gas before entering the injector. This was done to approximate the inlet hydrogen temperature which could be expected in a regeneratively-cooled system.

The chlorine trifluoride system was mounted on the thrust carriage close to the injector. Chlorine trifluoride was injected into the igniter chamber, as a liquid, through a single central orifice. Sufficient was contained in a small tank to complete eight ignitions. During a firing sequence the chlorine trifluoride tank was pressurized from its own nitrogen gas accumulator. This was an expedient to keep the remaining nitrogen gas system free of chlorine trifluoride, the latter having a nasty habit of diffusing through the system to gum up pneumatic valves. Hydrogen was taken from a standard gas cylinder and fed into the igniter through four radial holes, to impinge on the single chlorine trifluoride jet.

Figure 4 is a general view of the combustion test cell showing the disposition of some of the major components.

3.0 SEQUENCE OF OPERATION

The system was fully automatic as shown in Figure 5 and designed so that loss of electrical power caused a fail-safe condition. Since the duration of firing was short and the propellant feed lines long, it was necessary to pre-cool some of the system to guarantee a repeatable, crisp start-up. Therefore the pre-firing procedure included pre-cooling the liquid oxygen feed line through the injector and, also, pre-cooling the main hydrogen feed valve. Both these operations were done with liquid nitrogen.

Closure of the firing switch pressurized the oxygen and hydrogen tanks, started the cooling water flow and the injector purges. After a 4-second delay to stabilize the tank pressures the contacts of time-delay switch (T.D.2) closed and, consequential to the water flow having been established to make the contacts of pressure switch (P.1), the main hydrogen flow started. The resulting pressure rise in the hydrogen injector closed the contacts of pressure switch (P.2). This started the igniter and opened the oxygen valve, in the process shutting off the two injector purges. The igniter ran for 1.40 seconds then time-delay switch (T.D.1) contacts opened to shut it off. Twenty-five seconds after the oxygen valve had opened, time-delay switch (T.D.3) contacts broke to terminate combustion; other contacts on the same switch made to energize time-delay switch (T.D.4). Contacts on time-delay switch (T.D.4) broke 1.5 seconds later to shut off the main hydrogen valve and depressurize both propellant tanks. The firing switch was then opened to reset the system for the next firing.

An emergency stop button was also installed to terminate combustion if necessary during the timed sequence.

4.0 INSTRUMENTATION

All measurements were recorded on a 40-channel digital data acquisition system that was capable of printing 20 channels per second. Some data were recorded in parallel on a 6-channel oscillograph recorder with instant read-out for diagnostic purposes. A typical recording of the latter is shown in Figure 6. Both recorders were running continuously during the firing, the digital system measuring one complete set of data per second. For performance calculations the average of three consecutive sets of data was used.

Combustion pressure was measured by a strain gauge transducer that had both input and output voltages recorded on the data system.

Propellant and water flows were measured by turbine flowmeters, installed in each delivery line, whose outputs were recorded on both systems.

Thrust was measured, through a freely pivotting carriage, by a piezoelectric load cell.

Heat transfer was measured by copper/constantan thermocouples with an exposed bead to reduce the time constant. They were set in the coolant water stream at a distance of 0.030 inches from the combustion chamber wall. Measurements were taken at five stations along the chamber profile, see Figure 7. So that irregularities of stream temperature could be averaged out, four equally spaced thermocouples were placed at each station. The number of thermocouple measurements made on any one firing was twelve. Readings were made at Stations 1 and 5 on all firings, the other measurements floating between Stations 2, 3 and 4.

Hydrogen gas inlet temperature was measured with a platinum resistance thermometer installed in the main inlet pipe.

5.0 DISCUSSION OF RESULTS

Combustion Efficiency

In order to achieve an efficient low-pressure combustion system it was decided to use one which had four swirl atomizers for the oxidizer and a plain orifice pattern for the fuel. This decision was based on the arguments that (1) the oxygen, being injected as a liquid, required good atomization and even distribution; (2) the hydrogen, being injected as a gas, presented a problem of distribution only.

Five different combinations of this system were tested, the results of which are shown in Table I. Details of the various hole patterns are shown in Figure 8.

To evaluate the performance of the injector/combustion chamber combinations it was decided to use the parameter C* (characteristic velocity). This method measures performance on the basis of heat energy conversion only and does not require a knowledge of nozzle performance. Since our low combustion chamber pressure did not require a very large nozzle to expand the gases to atmospheric pressure it was considered an advantage to be able to ignore expansion cone losses.

A theoretical value of C* can be obtained from the expression

$$C^* = \frac{\sqrt{g \gamma R_1 / m \; T_c}}{\gamma \sqrt{\left[\frac{2}{\gamma + 1}\right]^{\frac{\gamma+1}{\gamma-1}}}} \tag{1}$$

where it can be seen that it is dependent upon combustion temperature (T_c), molecular weight of gas products (m) and the specific heat ratio of gas products (γ). These can all be evaluated during heat balance calculations at the design stage. For the purpose of our performance calculations theoretical values of C*, assuming frozen composition, were taken from data published by NASA [6].

Characteristic velocity can also be expressed by the equation

$$C^* = \frac{g \; p_o \; A_t}{\bar{w}} \tag{2}$$

which is a very convenient method of obtaining practical values, since it requires only the measurement of combustion pressure (p_o) and the total propellant flow ($\bar{w}$).

Evaluation of C* efficiency requires some adjustment to the theoretical value of C*. The theoretical data used [6] are calculated on the supposition that the hydrogen is liquid when injected into the combustion chamber. The hydrogen used in our experiments entered the combustion chamber at approximately 50°K (see Table I). The cooling water was also responsible for heat being irretrievably lost to the combustion process. The change in theoretical combustion temperature caused by the enthalpy gain of the former and the enthalpy loss of the latter, can be expressed by

$$\Delta T_c = \frac{\Delta H_h - \Delta H_c}{\bar{w} \; Cp}$$

It can be seen from Equation (1) that for a given mixture ratio, C* would vary in accordance with $\sqrt{T_c}$ then the C* correction factor = $\frac{\sqrt{Tcc}}{\sqrt{T_c}}$

Performance calculations of an ideal rocket chamber are based on the premise that combustion takes place at constant pressure, which can be considered true if the combustion zone gas velocity is near zero. In practice, there is a loss of energy between the injector face and the nozzle entry and, since we measured the combustion pressure at the injector face p_i, a correction was needed when evaluating C^*_A [7]. The momentum equation for frictionless flow in a constant area duct, assuming that $M_i \cong 0$ is given by

$$p_i = p_c \; (1 + \gamma M c^2)$$

and the relation for stagnation pressure is

$$p_o = p_c \left(1 + \frac{\gamma-1}{2} Mc^2\right)^{\frac{\gamma}{\gamma-1}}$$

then by substitution

$$p_o = p_t \frac{\left(1 + \frac{\gamma-1}{2} Mc^2\right)^{\frac{\gamma}{\gamma-1}}}{\left(1 + \gamma Mc^2\right)} \qquad (3)$$

and this calculation should be made for each firing. However, during the firings made we found that γ varied by less than one percent. Then by using the following equation and an average value for γ (1.218).

$$\frac{A_c}{A_t} = \frac{1}{Mc} \left(\frac{1 + \frac{\gamma-1}{2} Mc^2}{\frac{\gamma+1}{2}} \right)^{\frac{\gamma+1}{2(\gamma-1)}}$$

$$Mc = 0.103$$

then by substituting in Equation (3)

$$p_o = 0.9936\ p_t$$

This correction was used when evaluating C^*_A.

The following results were obtained:

Injector R.469/1

The oxygen swirl jets each had an included spray cone angle of 85°. Hydrogen was injected through the hole pattern shown in Figure 8a.
Combustion efficiency was 94.55%.

Injector R.469/2

The oxygen swirl jets each had an included spray cone angle of 110°. Hydrogen was injected through the hole pattern shown in Figure 8a.
Combustion efficiency was 96.47%.

Injector R.469/3

The oxygen swirl jets each had an included spray cone angle of 110°. Hydrogen was injected through the hole pattern shown in Figure 8b.
Combustion efficiency was 99.21%.

Injector R.470

The oxygen swirl jets each had an included spray cone angle of 110°. Hydrogen was injected through the hole pattern shown in Figure 8c.
Combustion efficiency was 98.85%.

Injector R.479

The oxygen swirl jets each had an included spray cone angle of 110°. Hydrogen was injected through the hole pattern shown in Figure 8d.
Combustion efficiency was 94.37%.

Note: The excessive values of C* efficiency for firings 92 and 107 are attributed to the accumulation of inaccuracies in measurement and correction factors.

TABLE I

RECORDS OF FIRINGS (PHASE I)

Firing No.	ΔH_c	Tgi	$\bar{w}$	O/F	p_i	p_h	p_{ox}	C^*_c	C^*_A	C^*_A/C^*_c%
					R.469/1					
53	88.815	46	1.3451	4.68	61.1115	36	47	7513	7129	94.90
54	82.137	47	1.3381	4.66	60.337	36	46	7527	7076	94.01
55	81.623	47	1.3445	4.81	60.5986	33	46	7481	7073	94.54
56	87.352	47	1.3165	4.61	59.881	36	44	7533	7138	94.75
					R.469/2					
57	102.494	44	1.3222	4.75	60.6771	33	43	7473	7201	96.36
58	98.333	48	1.3275	4.69	61.6133	33	42	7501	7283	97.10
60	97.019	46	1.3113	4.44	61.1951	32	39	7573	7323	96.70
62	97.395	48	1.3012	4.66	60.0672	35	40	7510	7244	96.46
63	97.737	48	1.3044	4.59	60.5859	35	39	7530	7288	96.78
64	101.641	49	1.2993	4.90	59.8394	34	40	7430	7227	97.28
65	98.365	47	1.3359	4.73	61.646	31	44	7489	7241	96.69
66	97.665	45	1.3308	4.57	61.9671	27	41	7535	7307	96.97
67	97.987	47	1.3427	4.68	62.2985	31	42	7504	7281	97.02
68	98.771	44	1.3386	4.70	61.2351	31	41	7495	7178	95.77
69	101.110	47	1.3366	4.64	61.7624	32	41	7513	7251	96.51
70	98.879	46	1.3516	4.62	61.335	33	41	7521	7121	94.68

TABLE I (Cont'd)

Firing No.	ΔH_c	Tgi	$\bar{w}$	O/F	p_i	p_h	p_{ox}	C^*_c	C^*_A	C^*_A/C^*_c %
					R.469/2 (Cont'd)					
71	103.344	44	1.3363	4.66	61.2884	31	40	7504	7197	95.91
72	111.685	47	1.3382	4.77	61.7924	32	40	7463	7246	97.09
73	102.796	45	1.3425	4.70	61.2471	33	40	7492	7159	95.55
76	102.706	46	1.3459	4.74	61.7813	33	39	7481	7203	96.28
77	112.520	47	1.3398	4.71	61.4265	33	39	7482	7194	96.16
78	100.730	41	1.3521	4.57	62.4276	31	39	7532	7245	96.20
79	104.200	47	1.3210	4.70	61.4145	33	40	7491	7295	97.39
					R.469/3					
80	121.044	45	1.3005	4.54	61.5864	31	40	7518	7431	98.84
81	122.933	44	1.3055	4.51	61.8937	31	41	7526	7440	98.86
83	122.838	49	1.3260	5.10	62.0334	34	37	7351	7341	99.86
84	130.938	49	1.2803	4.86	59.5946	34	35	7413	7304	98.53
85	148.115	47	1.3072	4.85	60.8935	35	35	7401	7310	98.77
86	132.277	47	1.3381	4.85	62.5178	36	37	7419	7332	98.82
90	116.941	48	1.2979	4.80	60.7460	35	36	7445	7344	98.65
91	117.809	50	1.2937	4.92	60.6823	36	34	7410	7361	99.34
92	121.640	47	1.3074	4.61	62.7515	29	34	7498	7532	100.45
93	131.054	49	1.2782	4.80	60.5192	32	34	7431	7430	99.98
					R.470					
97	127.066	47	1.3005	4.56	61.4696	28	41	7508	7417	98.79
98	119.950	49	1.3076	4.74	61.3807	32	43	7464	7366	98.69
100	127.205	47	1.3307	4.81	61.4778	31	43	7437	7250	97.48
102	124.175	47	1.3159	4.70	61.0672	31	40	7471	7282	97.47
103	126.578	49	1.3076	4.76	60.7175	33	40	7452	7287	97.78
104	127.166	51	1.3010	4.84	60.9868	33	40	7427	7356	99.05
105	124.788	53	1.3024	4.82	60.9129	32	40	7435	7339	98.71
107	117.799	49	1.2982	4.75	61.8691	30	41	7460	7479	100.25
109	122.306	50	1.3013	4.71	60.8702	32	40	7470	7340	98.27

TABLE I (Cont'd)

Firing No.	ΔH_c	Tgi	$\bar{w}$	O/F	p_i	p_h	p_{ox}	C_c^*	C_A^*	C_A^*/C_c^* %
					R.470 (Cont'd)					
110	128.885	57	1.3039	4.90	61.4398	33	41	7409	7394	99.81
111	135.182	49	1.2924	4.50	61.6274	27	39	7519	7483	99.52
112	128.357	49	1.2953	4.63	59.4415	30	40	7486	7201	96.19
113	127.519	49	1.2808	4.69	60.0691	30	39	7469	7360	98.54
114	120.152	50	1.2933	4.65	61.4629	30	39	7488	7458	99.60
115	118.433	49	1.2849	4.63	61.1541	30	38	7496	7469	99.64
116	122.605	50	1.2933	4.68	61.4322	31	38	7479	7454	99.67
117	118.354	50	1.3076	4.71	61.9653	31	38	7474	7436	99.49
118	121.764	50	1.2959	4.58	61.7913	32	37	7507	7482	99.67
119	118.346	48	1.2950	4.67	61.5150	34	38	7484	7454	99.60
					R.479					
121	86.813	50	1.2894	4.39	59.2748	18	43	7597	7214	94.95
122	84.174	49	1.3167	4.47	59.8773	18	44	7579	7136	94.15
123	103.956	50	1.3107	4.89	56.9088	22	46	7434	6813	91.65
124	102.021	50	1.3234	4.67	61.0639	19	44	7503	7241	96.50
125	100.486	49	1.3289	4.65	56.7944	23	46	7510	6707	89.30
128	108.813	48	1.3603	4.49	62.6166	17	43	7552	7223	95.65
129	104.882	49	1.3451	4.80	61.6991	17	44	7463	7198	96.45
130	90.977	49	1.3309	4.79	60.5590	21	43	7478	7140	95.49
131	102.742	48	1.3356	4.73	61.1718	22	43	7485	7187	96.02
132	105.226	49	1.3569	4.61	60.6888	17	43	7520	7019	93.33
133	99.957	50	1.3633	4.68	61.3889	17	43	7506	7066	94.14
134	99.607	46	1.3373	4.64	60.7045	20	43	7514	7123	94.80

Calculation of Heat Transfer in a Rocket Combustion Chamber

Heat is transferred from the combustion gases to the chamber wall principally by forced convection and can be expressed by the equation

$$q_1 = h_g \ (Taw - Twg) \qquad (a)$$

Evaluation of the hot gas film coefficient (h_g) is a rather complex problem and has been the subject of much study. For our investigation we have used an equation developed by Bartz[8]

$$h_g = \left[\frac{0.026}{D_t^{0.2}} \left(\frac{\mu^{0.2} C_p}{P_r^{0.6}} \right) \left(\frac{p_c\, g}{C^*} \right)^{0.8} \left(\frac{D_t}{R} \right)^{0.1} \right] \left(\frac{A_t}{A} \right)^{0.9} \sigma \qquad \text{(b)}$$

where $$\sigma = \frac{1}{\left[0.5 \frac{Twg}{T_c} \left(1 + \frac{\gamma - 1}{2} M_c^{\,2} \right) + 0.5 \right]^{0.68} \left[1 + \frac{\gamma - 1}{2} M_c^{\,2} \right]^{0.12}}$$

Using previously calculated combustion data[6] and assuming frozen composition Equation (b) can be rewritten

$$h_g = 0.0523 \left(\frac{A_t}{A} \right)^{0.9} \sigma \qquad \text{(c)}$$

It can be seen that evaluation of σ for a given area ratio $\left(\frac{A_t}{A} \right)$ requires prior knowledge of the value Twg, which we do not have. It is therefore necessary to construct curves of σ against Twg for different values of $\left(\frac{A_t}{A} \right)$ to aid the iteration process used later.

Heat transfer through the chamber wall can be expressed by the general equation

$$q_2 = \frac{k}{t} (Twg - Twc)$$

Similarly heat transfer from the chamber wall to the coolant can be written

$$q_3 = h_c (Twc - Tco)$$

Now when considering multilayer heat transfer through a flat plate $q_1 = q_2 = q_3$ but in a combustion chamber where the surfaces are curved we must consider the difference in areas.

If we let a_1 = inside wall surface area

a_2 = outside wall surface area

then $$q_1 a_1 = q_3 a_2$$

or $$q_3 = q_1 \frac{a_1}{a_2}$$

and similarly $$q_2 = q_1 \frac{2a_1}{a_1 + a_2}$$

then $$q_1 = h_g \ (Taw - Twg) \qquad (d)$$

$$q_1 = \frac{a_1 + a_2}{2a_1} \left(\frac{k}{t}\right) \ (Twg - Twc) \qquad (e)$$

$$q_1 = \frac{a_2}{a_1} \ h_c \ (Twc - Tco) \qquad (f)$$

The behaviour of water as a coolant is well known[9], a simplified equation for the water film coefficient

$$h_c = 2.15 \times 10^{-3} \ (1 + 0.015 \ Tco) \ Vco^{0.8} \ D^{-0.2} \qquad (g)$$

This equation is also valid for water flowing in annular spaces if $(D_1 - D_2)$ is substituted for D, and holds good whether heat is flowing through one or both of the wetted surfaces.

Then for a given area ratio $\frac{A_1}{A}$, having evaluated Equation (g), a temperature Twg can be assumed which allows the evaluation of Equation (c) and the subsequent balancing of Equations (d) (e) and (f) by the process of iteration. Repeating this process for different values of $\frac{A_1}{A}$ obtains heat transfer rates and water coolant temperatures along the profile of the combustion chamber.

Having obtained the theoretical values these can then be compared with the actual values measured in order to gain some knowledge of the conditions produced by the different injectors.

Table II shows the amount of heat absorbed by the cooling water expressed as a percentage of the total and is the result of the collation of 51 firings. It can be seen that in all cases more than 90% of the heat was absorbed prior to Station 4. This table also shows that when injector efficiency was the highest the amount of heat transferred in the throat region (Stations 4 - 5) was the lowest.

Table III shows a comparison between the actual percent heat transferred and the theoretical percent heat transferred. It also shows the ratio of measured total heat to water against the theoretical total heat to water and it can be seen that this ratio clearly reflects the injector efficiencies.

The lower than predicted total heat transferred could partly be explained by a coating which built up on the inside of the combustion chamber. This layer was formed by the presence of a small amount of chlorine trifluoride gas which lingered in the

combustion chamber after each firing. Examination of this film on the completion of experiments showed it to be very tough and it could have acted as a partial insulator. The low heat transfer ratio in the throat region could be explained in part by the higher than usual combustion zone length/diameter ratio used. We adopted a ratio of 2 to 1 so that we could more easily observe the effect of the injectors on heat transfer in this zone, but a more usual ratio would be 1.25 to 1.

TABLE II

HEAT TRANSFER PROFILE

(% heat gained by water)

Stations	1-2	2-3	3-4	4-5
R.469/2	40.23	23.05	28.20	8.52
R.469/3	33.50	32.67	27.21	6.62
R.470	28.20	34.14	31.04	6.62
R.479	24.17	30.97	35.54	9.32

TABLE III

HEAT TRANSFER

(% of theoretical)

Stations	1-2	2-3	3-4	4-5	1-5
R.469/2	147.04	84.28	107.51	44.70	79.30
R.469/3	122.44	119.45	103.74	34.73	96.75
R.470	103.07	124.83	118.34	34.73	95.22
R.479	88.34	113.24	135.49	48.90	75.83

Mechanical Reliability

This system was operated over a 2-year period under ambient conditions which ranged from a maximum temperature of 87° F to a minimum temperature of -2° F; at times the humidity was 100%.

A total of 88 firings were attempted with the same combustion chamber, of these 15 were non-firings. However, none of the latter could be attributed to the ignition

principle used, i.e. hypergolic ignition of chlorine trifluoride and hydrogen, since they were all due to mechanical faults which were cured.

The main causes of failure were:

Liquid oxygen feed valve which was a proprietary valve that had been modified to give it a double-acting actuator. It had a rather rigorous performing cycle since it was opened 10 minutes before the firing to allow pre-cooling liquid nitrogen through it, closed immediately before the firing commenced; then it had to open during the automatic start sequence and close again 25 seconds later. During days of high humidity this valve was prone to freeze up when subjected to its low operating temperature. On days such as this a warm gas system was used to dry out the valve before use.

Chlorine trifluoride feed valve initially had teflon lip seals on the operating shaft which would "gum-up" occasionally when corrosion products coated the shaft. A valve was designed and made with a bellows seal and a double-acting piston which proved to be a very reliable replacement.

Hydrogen igniter feed valve also developed a sticky shaft seal which was cured by a similar valve to the one above.

Chlorine trifluoride safety diaphragm was subjected to sudden pressurization during the firing cycle and a vacuum pressure during the fill cycle. This caused fatigue failures of the diaphragm material resulting in loss of the chlorine trifluoride. Once the reliable working life of the diaphragm was established the problem was solved by isolating it from vacuum pressure with a hand valve, and changing the burster material at regular intervals.

The above items were responsible for 87% of the non-firings, which is a good indicator of the reliability of the remainder of the system.

HYDROGEN-COOLED COMBUSTION CHAMBER

General Description

The stainless steel regeneratively-cooled combustion chamber was based on experience gained during Phase I. Unfortunately some deviations had to be made from the original chamber shape as a consequence of the physical limitations of the test site and available test equipment, the main limitation being on the maximum pressure which would be attained on the hydrogen system. The new chamber was therefore designed around the latter, resulting in a combustion chamber diameter of 4.00 inches, an oxygen/fuel ratio of 3.175 to 1, and a length/diameter ratio of 1.5 to 1. However, it was not thought that these changes would detract from the useful information gained from such a system.

The hydrogen-cooled combustion chamber shown in Figure 9 had a combustion pressure of 60 psia which expanded down to an exhaust pressure of 14.7 psia. The nominal thrust produced was 193 lb. The cooling hydrogen entered the chamber jacket at the injector end to flow longitudinally through an annular passage of constant height (0.062 in).

Two pipes transferred the hydrogen from the exhaust end to the injector, each pipe containing an expansion bellows. A sliding seal was fitted at the exhaust end of the chamber to allow free expansion of the inner liner. The injector pattern was similar to the most successful one used in Phase I and was constructed in stainless steel.

The complete system is shown schematically in Figure 10.

Sequence of Operation

An automatic system was again used as shown in Figure 11. The pre-firing procedure included pre-cooling the liquid oxygen feed line, and the main hydrogen valve, with liquid nitrogen.

Closure of the firing switch pressurized the liquid oxygen and liquid hydrogen tanks and began the nitrogen gas purges through the oxygen and hydrogen injectors. After a 4-second delay to stabilize the tank pressures, time-delay switch (T.D.2) contacts closed to initiate the following:

(a) main hydrogen flow through the combustion chamber jacket, injector and out to atmosphere;

(b) liquid oxygen flow as far as the oxygen feed valve, then out to atmosphere;

(c) shut off the nitrogen gas purge to the hydrogen injector.

Time-delay switch (T.D.4) contacts closed 7.5 seconds later to start the igniter, close the oxygen bypass valve, open oxygen feed valve and stop the nitrogen gas purge to the oxygen injector. After 1.40 seconds the igniter automatically shut off when time-delay switch (T.D.1) contacts broke. Time-delay switch (T.D.3) contacts broke to close the oxygen valve 10 seconds after the commencement of ignition, thus terminating combustion and the nitrogen purge re-established itself through the oxygen injector. The firing switch was then manually opened to shut down the remainder of the system and depressurize the tanks. An emergency stop button was installed to terminate combustion during the timed sequence.

Instrumentation

This was similar to that of Phase I except for temperature measurements.

Hydrogen coolant temperatures (inlet and outlet) were measured by platinum resistance thermometers whose outputs were recorded on the digital data system. An intermediate coolant temperature was also measured near the end of the combustion zone. This measurement was made by averaging out three equally spaced copper-constantan thermocouples of the exposed bead type, whose tips were 0.030 inches from the combustion chamber wall.

A typical recording made on the oscillograph for diagnostic purposes can be seen in Figure 12.

Discussion of Results

Twelve firings were made with this combustion chamber, the results of which are shown in Table IV.

TABLE IV

RECORDS OF FIRINGS (PHASE II)

Firing No.	ΔH_{ch}	Tgi	$\bar{w}$	0/F	p_i	p_h	p_{ox}	C^*_c	C^*_A	C^*_A/C^*_c%
1	81.337	64	0.7267	2.87	55.595	-	-	8011	7629	95.24
2	69.23	60	0.7087	2.58	54.879	-	-	8006	7722	96.46
3	80.974	64	0.7317	2.95	57.040	21	26	8005	7774	97.11
4	80.159	63	0.7502	3.01	57.441	22	27	7999	7636	95.46
5	85.748	64	0.7749	3.30	60.781	20	30	7961	7822	98.25
6	84.048	63	0.7847	3.18	61.287	19	25	7980	7789	97.60
7	89.189	62	0.7871	3.00	60.286	20	33	7999	7638	95.49
8	83.410	63	0.8045	3.35	61.081	19	35	7951	7571	95.22
9	73.113	62	0.8178	3.13	60.986	15	34	7984	7437	93.14
10	-	-	0.8155	3.24	61.047	16	35	7969*	7465	93.68
11	66.019	59	0.8291	3.20	61.739	14	34	7973	7426	93.14
12	75.146	60	0.8016	3.31	60.337	14	32	7956	7506	94.34

* estimated value

The first four firings were made at a lower than design mixture ratio in order to establish operating levels. As the design parameters were approached, there was a slight increase in C* efficiency and overall heat transfer (firings 5 to 8 inclusive). Coincident with this improvement, regions of excessive heat were observed along the chamber in line with each of the liquid oxygen swirl injectors (see Figure 13). There was no failure of the chamber wall. It was realised that the close proximity of the oxygen injectors to the chamber wall demanded efficient mixing to prevent oxygen-rich regions near the latter. The injector was modified in an attempt to correct this, by adding more hydrogen holes at the periphery. The modification was not successful; it merely reduced the combustion efficiency by about three percent. It is now believed that these hot regions can be prevented, and the combustion efficiency improved, by increasing the hydrogen injector pressure-drop (p_h). The (p_h) in this series of firings was substantially lower than that of the water-cooled series. A higher pressure drop would give the hydrogen a higher entrance velocity and consequently greater penetration. It was not possible to substantiate this belief, however, owing to the rig limitations already noted.

Examination of the overall heat transfer of each firing showed that steady state cooling conditions were reached after about six seconds into the firing. Since the chamber wall did not fail in the hot regions it is reasonable to assume that the cooling would be

adequate for a more homogeneous flame. However, the establishment of final cooling requirements would be consequential to achieving the desired combustion efficiency.

6.0 CONCLUSIONS

Our investigations showed that for the combustion configuration considered, viz. a 60 psia combustion pressure chamber with 500 lb thrust optimum expansion, a simple low-pressure injection system can be designed that will give an acceptable combustion efficiency.

We also demonstrated that it could be controlled by a reliable pressure-fed system using hypergolic ignition.

Preliminary work on a regeneratively-cooled combustion chamber, using a simple annular cooling passage, also indicated that this method of cooling might be successfully integrated in the above system.

7.0 REFERENCES

1. Ohman, L.H. — A Method for Satellite Launch Vehicle Performance Analysis with Application to Black Brant V-B. Sounding Rocket Motor Booster Configurations. NRC, Aeronautical Report LR-461, National Research Council of Canada, Ottawa, Ontario.

2. Ohman, L.H. — Canadian Aeronautics and Space Journal, Vol. 13, No. 9, November 1967, pp. 427-435.

3. Sandri, R. Billingham, R. — Experiments on Ignition of Bipropellants under Vacuum Conditions. I -- On Pyrotechnic Ignition of Ethyl Alcohol and Liquid Oxygen. NRC, Mech. Eng. Report MP-27, National Research Council of Canada, Ottawa, Ontario, May 1963.

4. Sandri, R. Billingham, R. — Ignition of the Hydrogen-Oxygen Propellant Combination by Means of Chlorine Trifluoride. AIAA Journal, Vol. 5, No. 4, April 1967, pp. 770-773.

5. Watson, E.A. — Fuel Systems for Aero Gas Turbines. Institution of Mech. Engineers (British) Proceedings 1948, Vol. 158, No. 2, pp. 195-199.

6. Gordon, S. McBride, B.J. — Theoretical Performance of Liquid Hydrogen with Liquid Oxygen as a Rocket Propellant. NASA Lewis Research Centre, Memo 5-21-59E, 1959.

7. Altman, D.
Carter, J.M.
Penner, S.S.
Summerfield, M.
Liquid Propellant Rockets.
Princeton University Press.

8. Huzel, D.K.
Huang, D.H.
Design of Liquid Propellant Rocket Engines.
NASA Publication SP-125, 1971.

9. Spiers, H.M.
(Editor)
Technical Data on Fuel.
British National Committee World Power Conference, 1952.

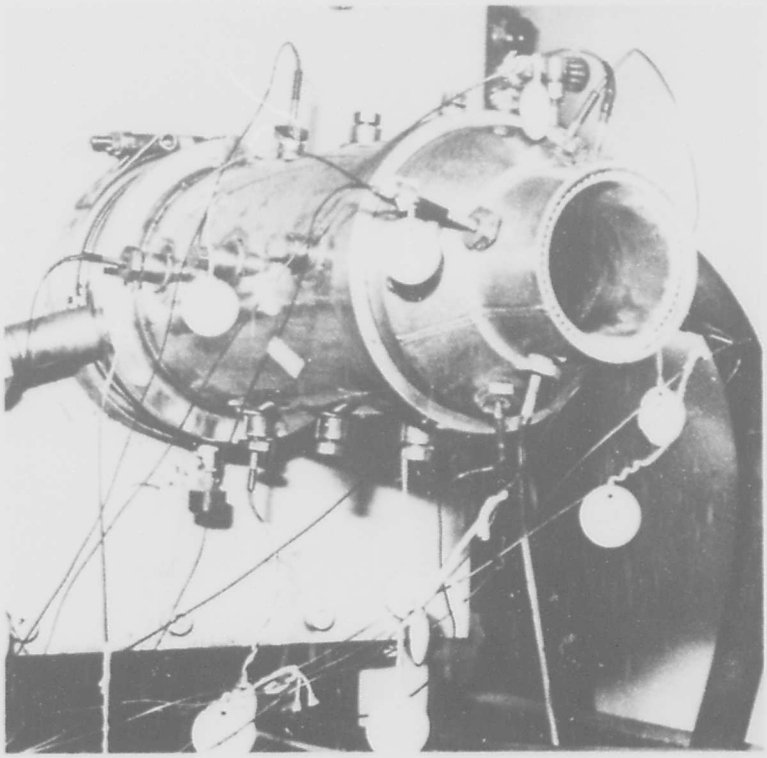

FIG. I : WATER-COOLED COMBUSTION CHAMBER

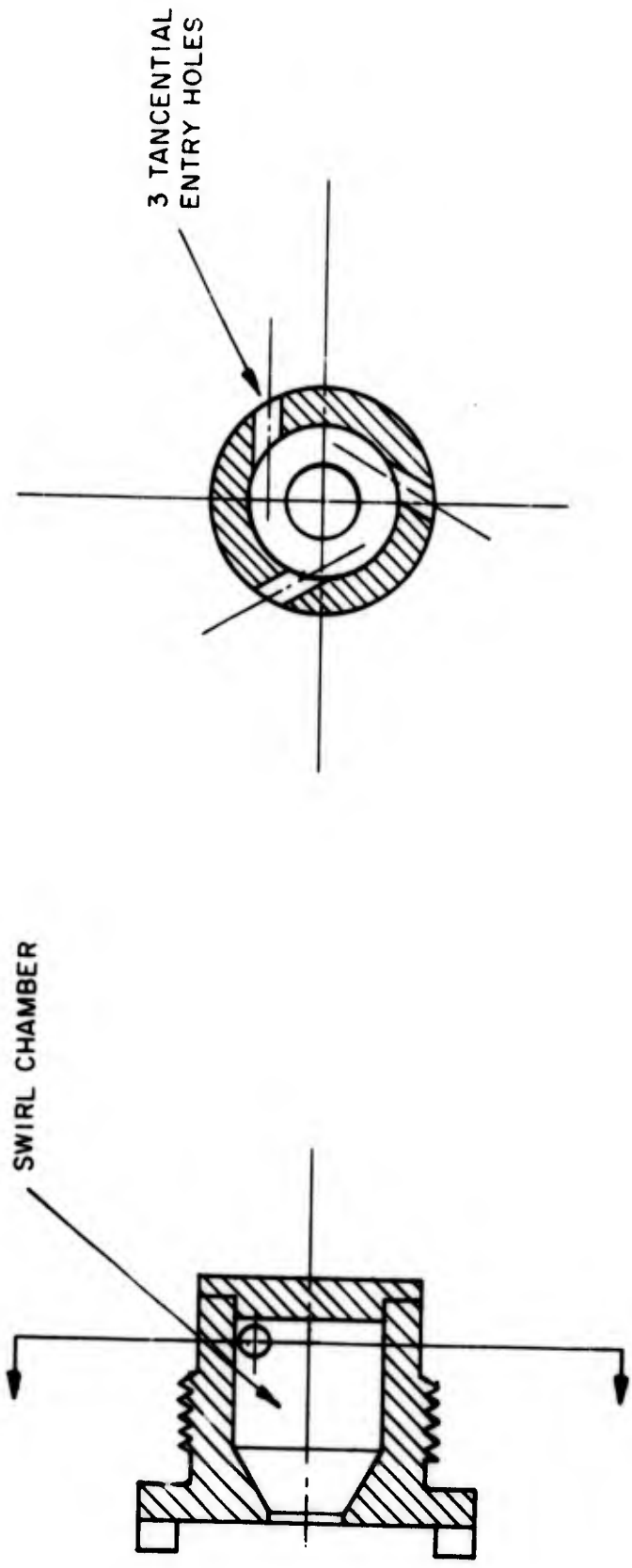

FIG.2 : LIQUID OXYGEN SWIRL ATOMIZER

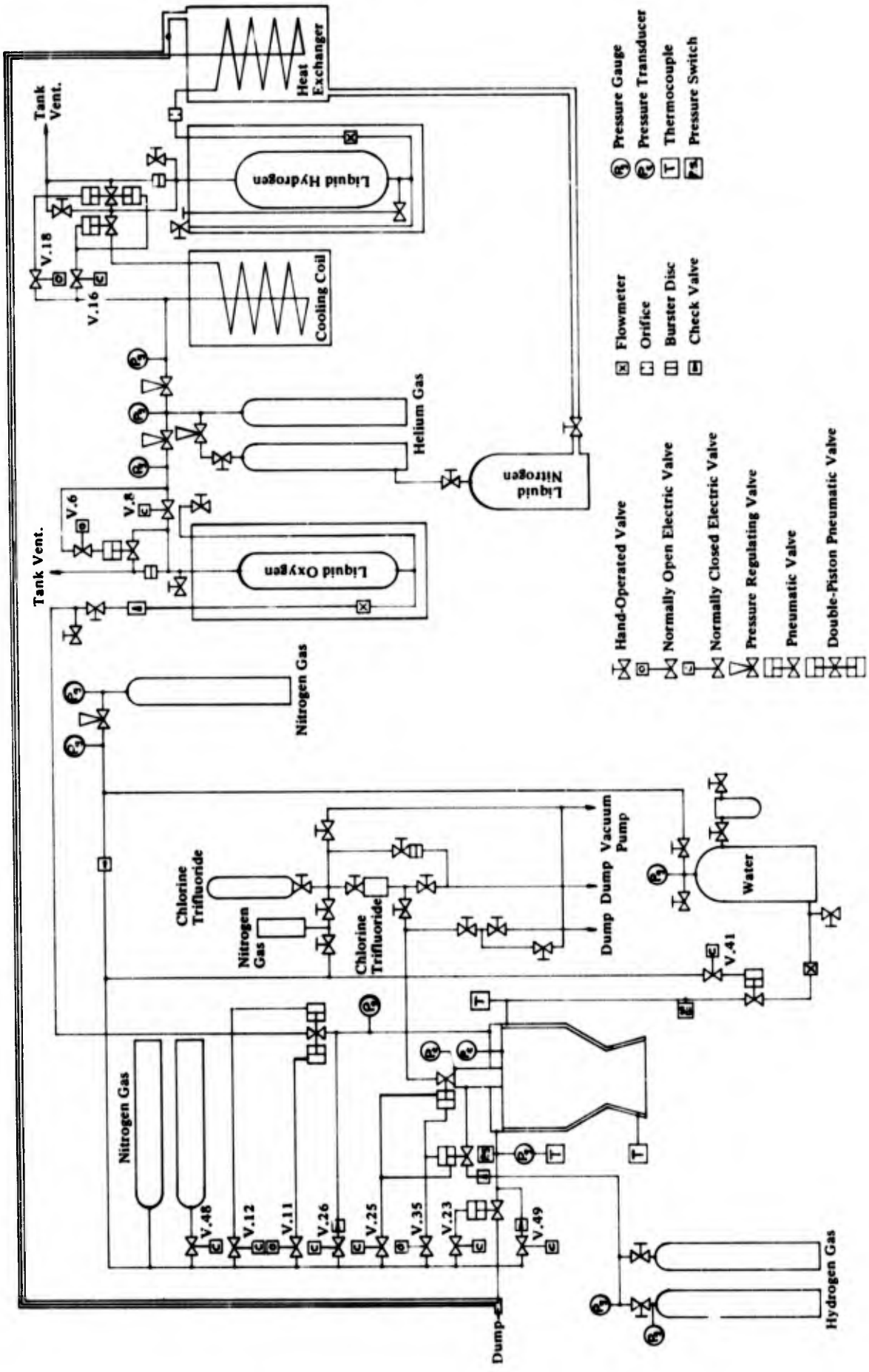

FIG. 3 : PROPELLANT FEED SYSTEM (SCHEMATIC) (PHASE I)

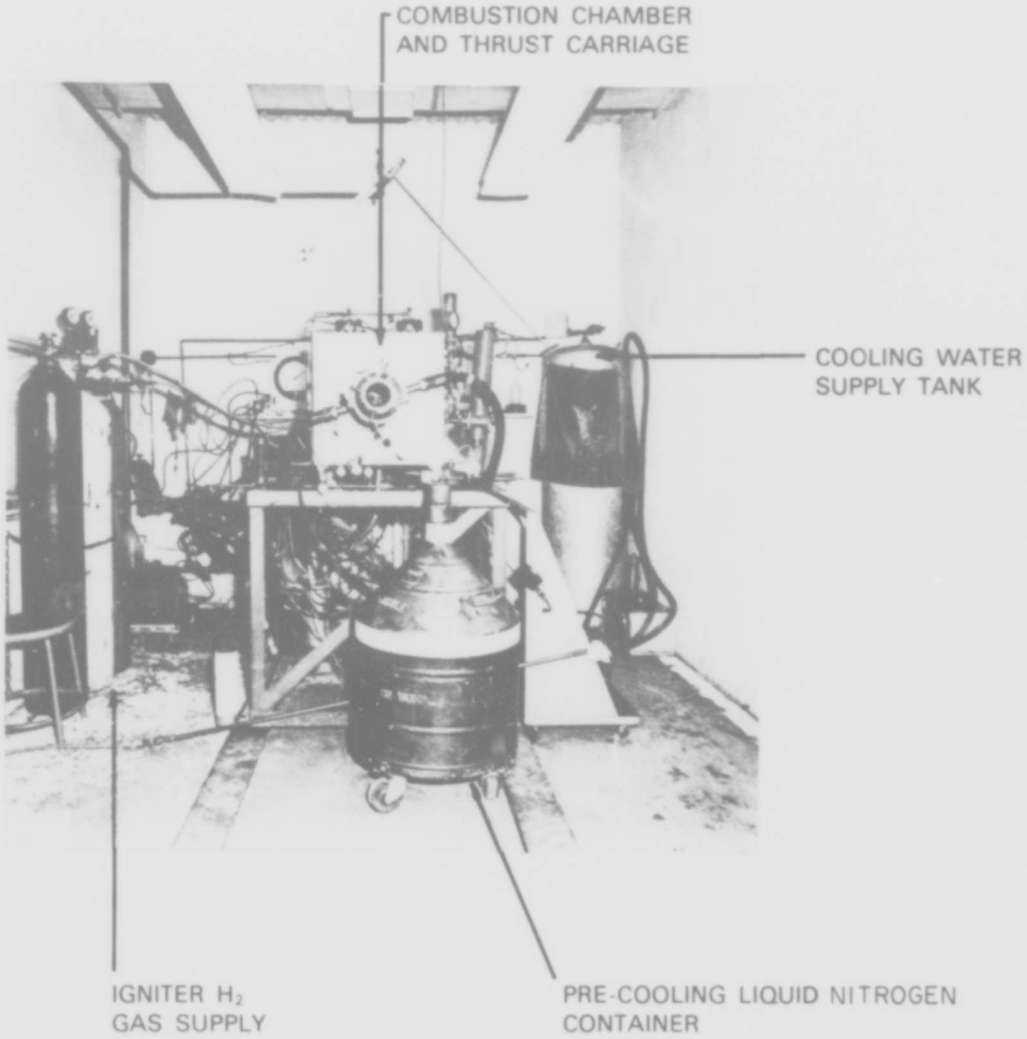

FIG. 4 : COMBUSTION TEST CELL

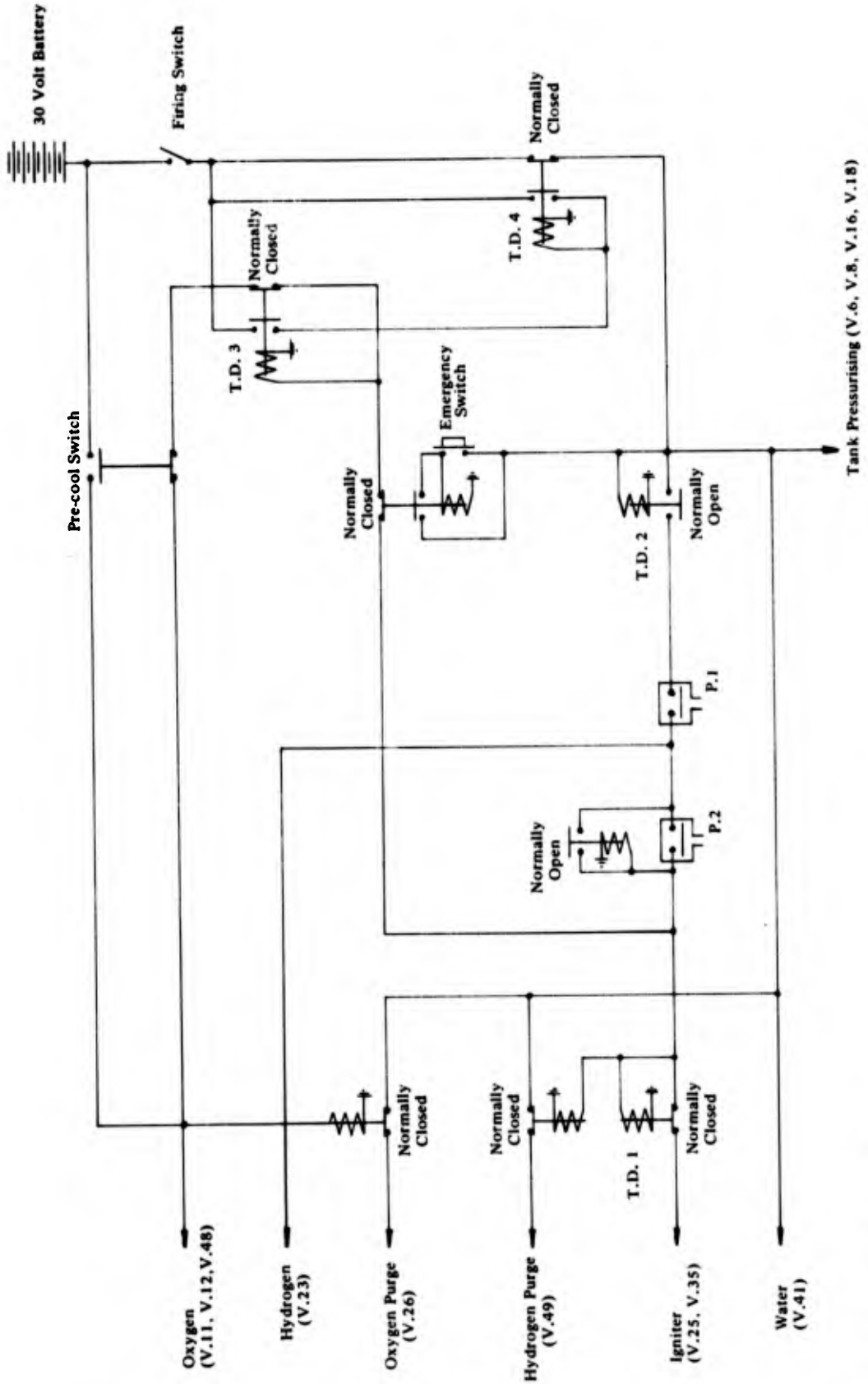

FIG.5 : AUTOMATIC CONTROL CIRCUIT (SCHEMATIC) (PHASE I)

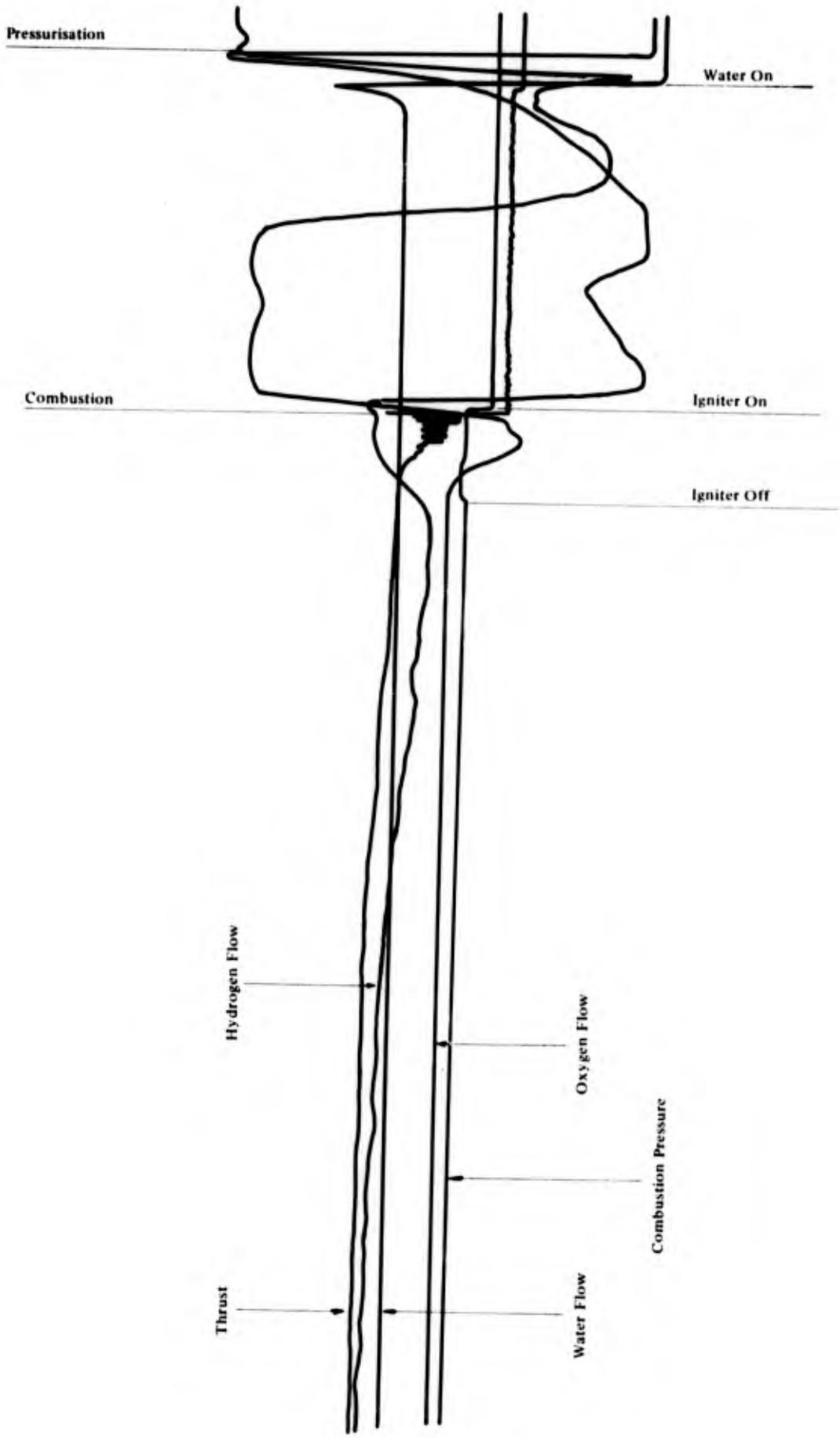

FIG. 6 : OSCILLOGRAPH RECORD OF EVENTS (FIRING NO. 122)

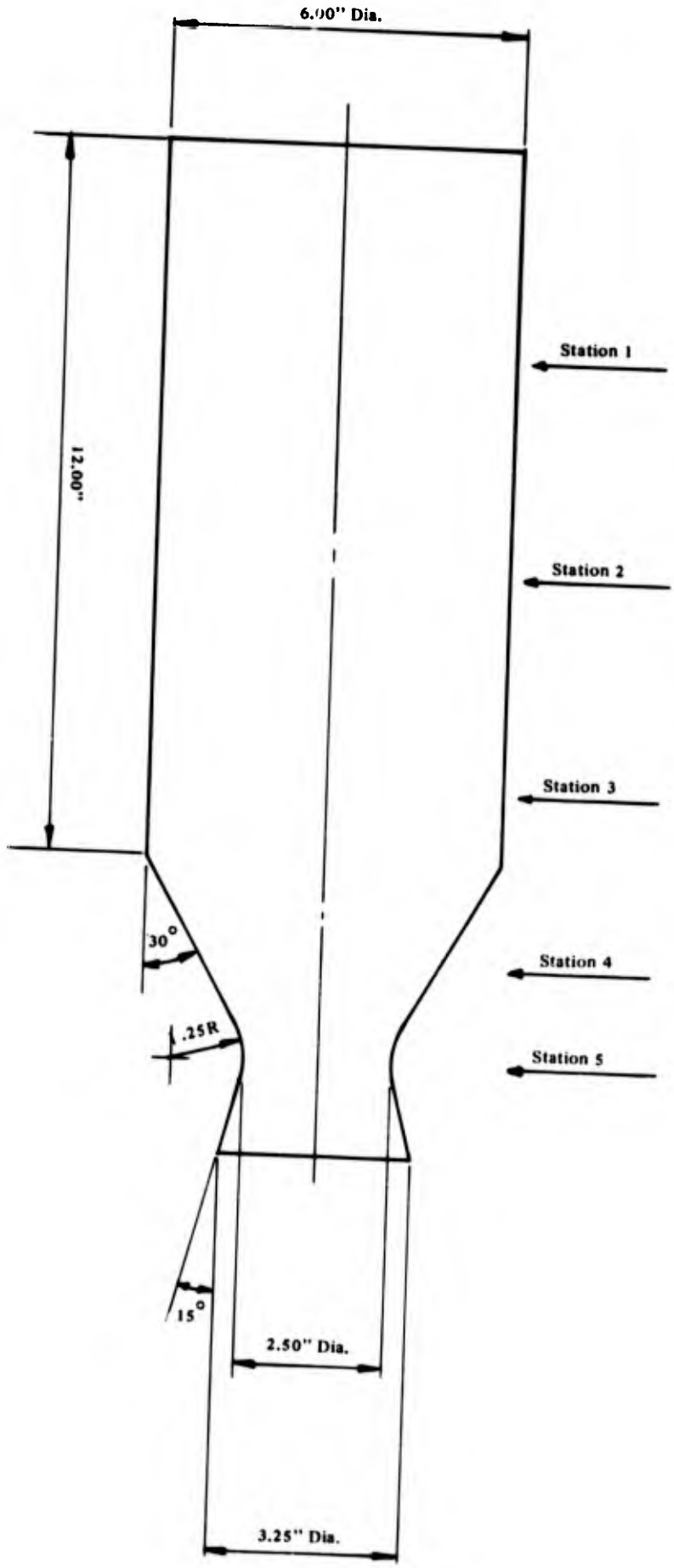

FIG. 7 : COMBUSTION CHAMBER PROFILE

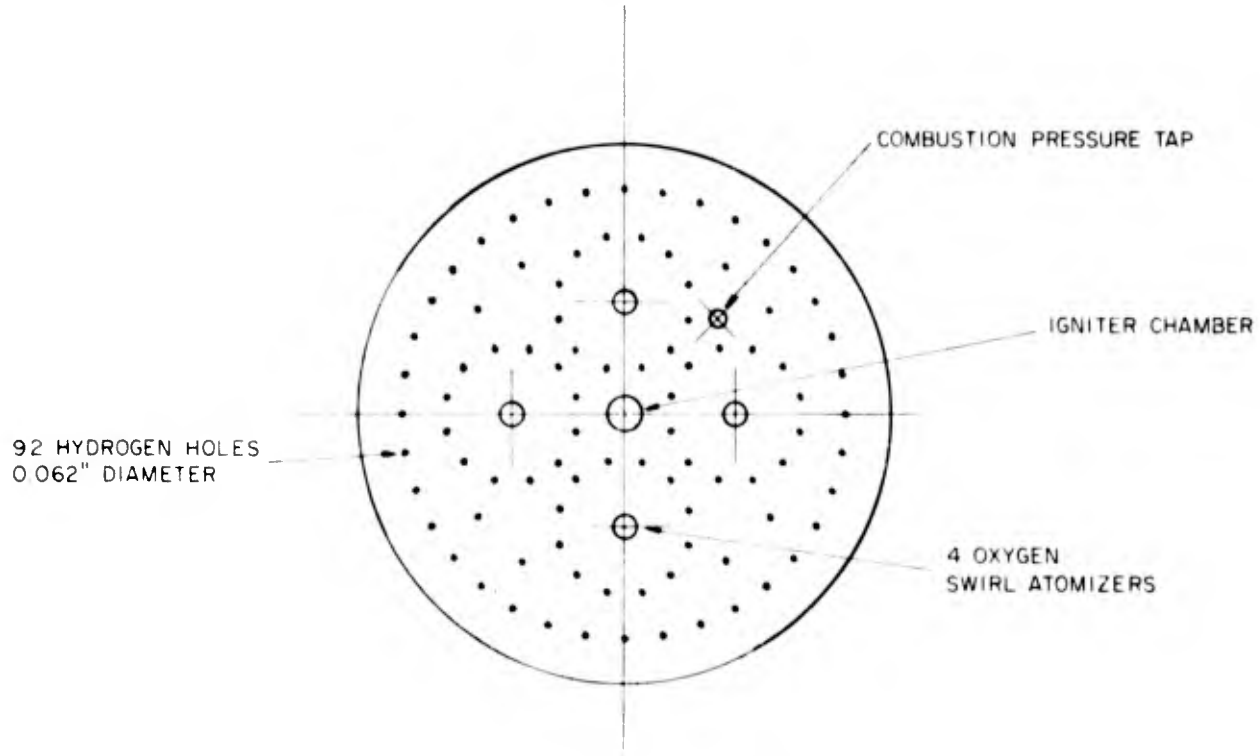

FIG. 8a : INJECTOR PATTERN

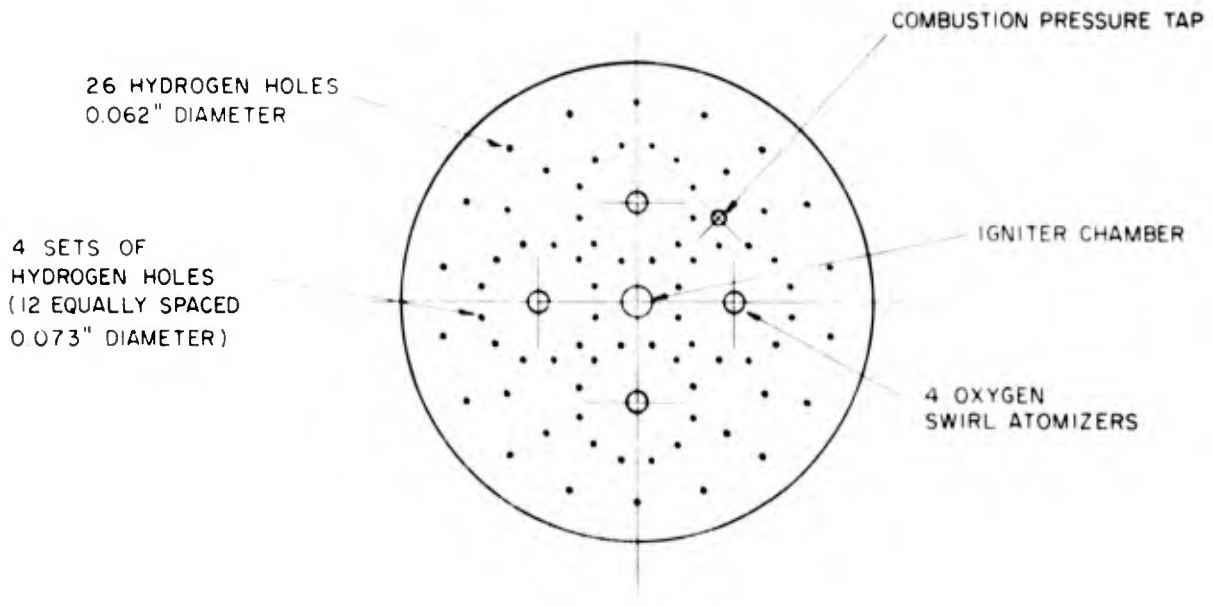

FIG. 8b : INJECTOR PATTERN

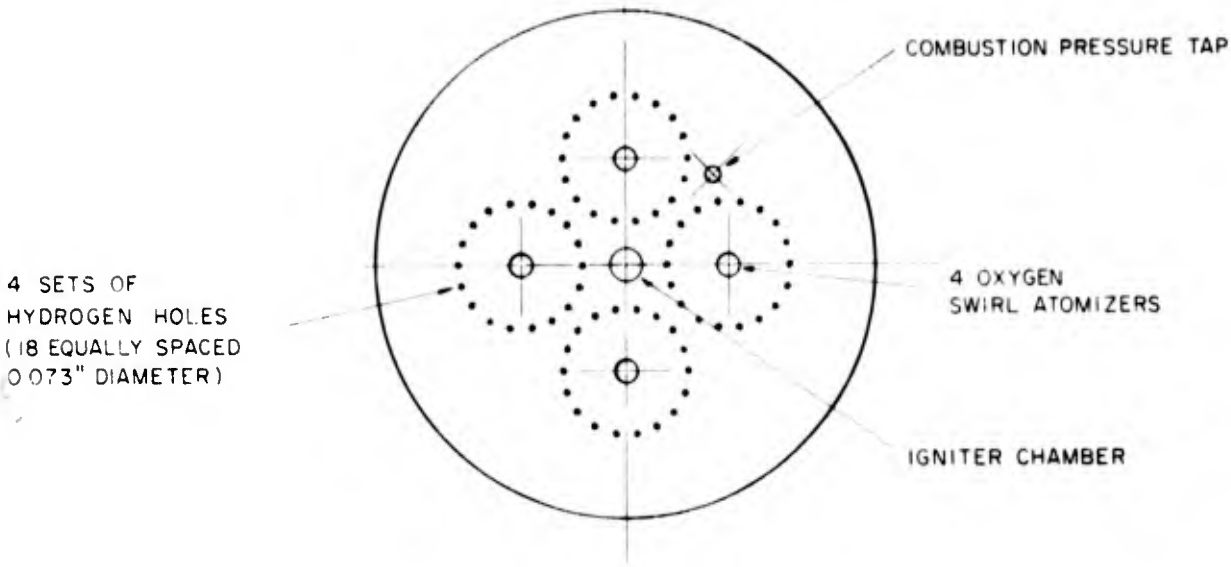

FIG. 8c : INJECTOR PATTERN

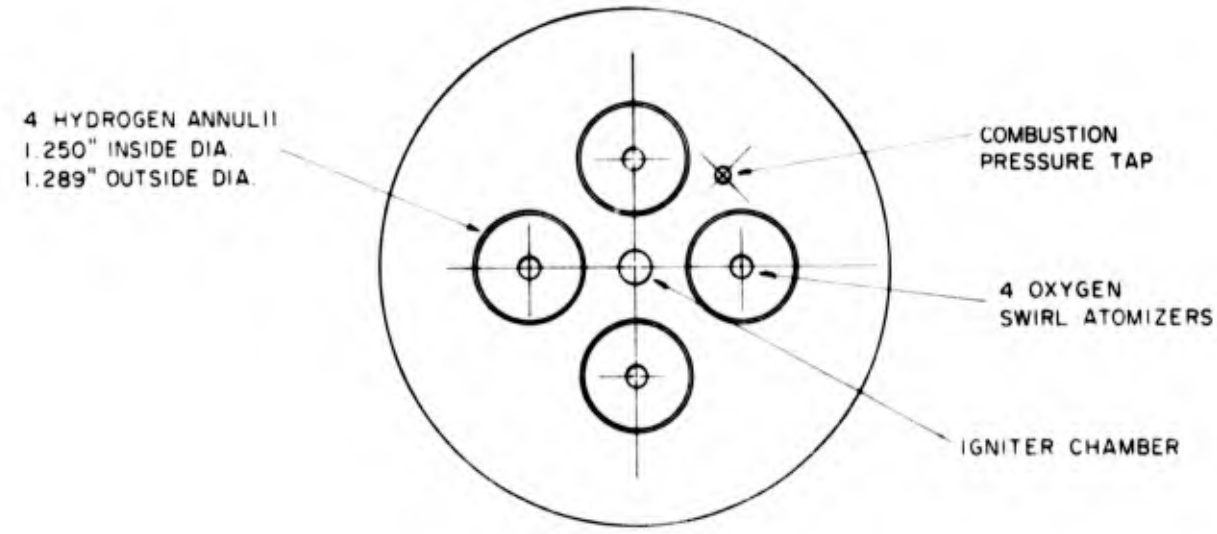

FIG. 8d : INJECTOR PATTERN

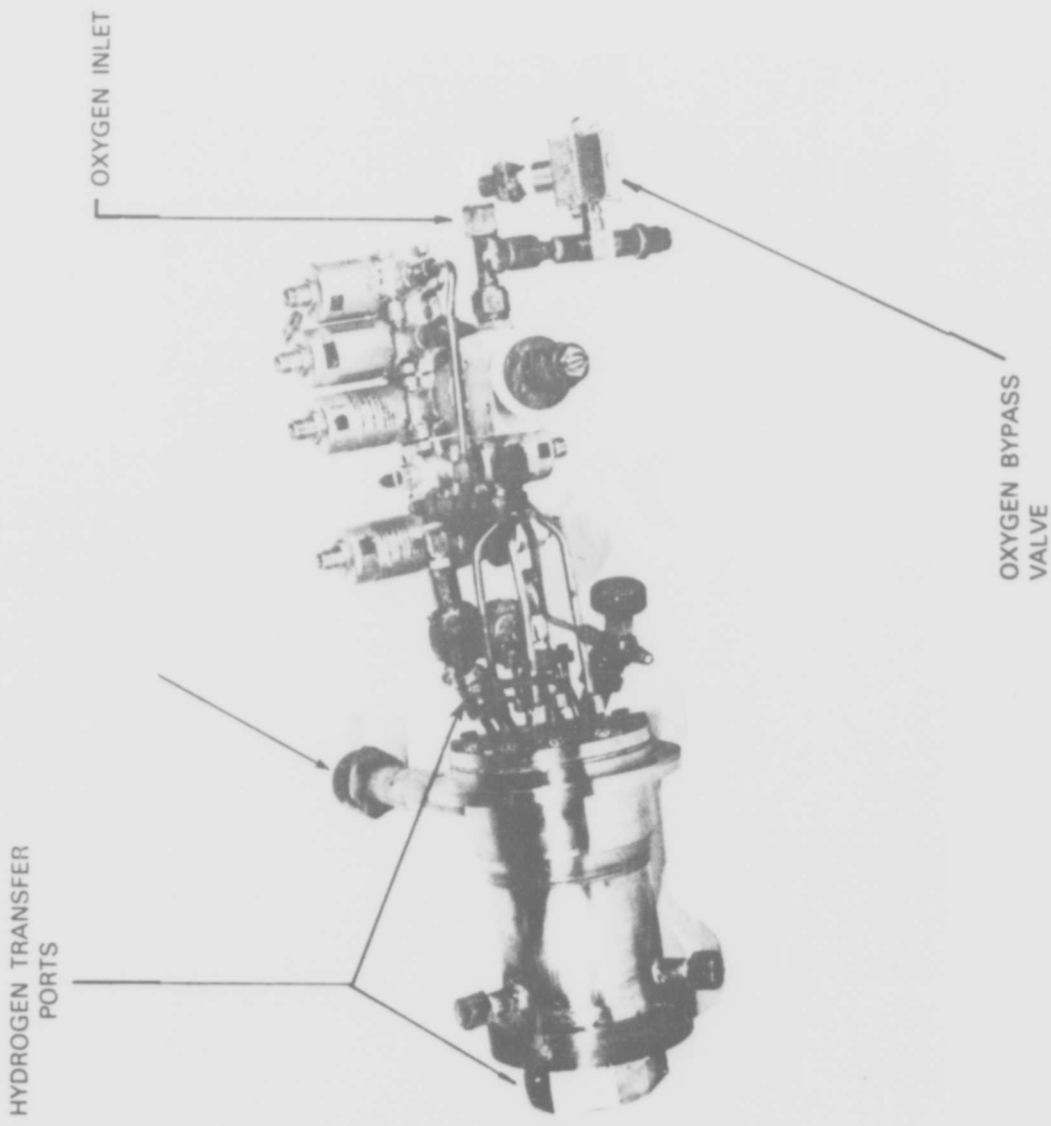

FIG. 9 : HYDROGEN-COOLED COMBUSTION CHAMBER

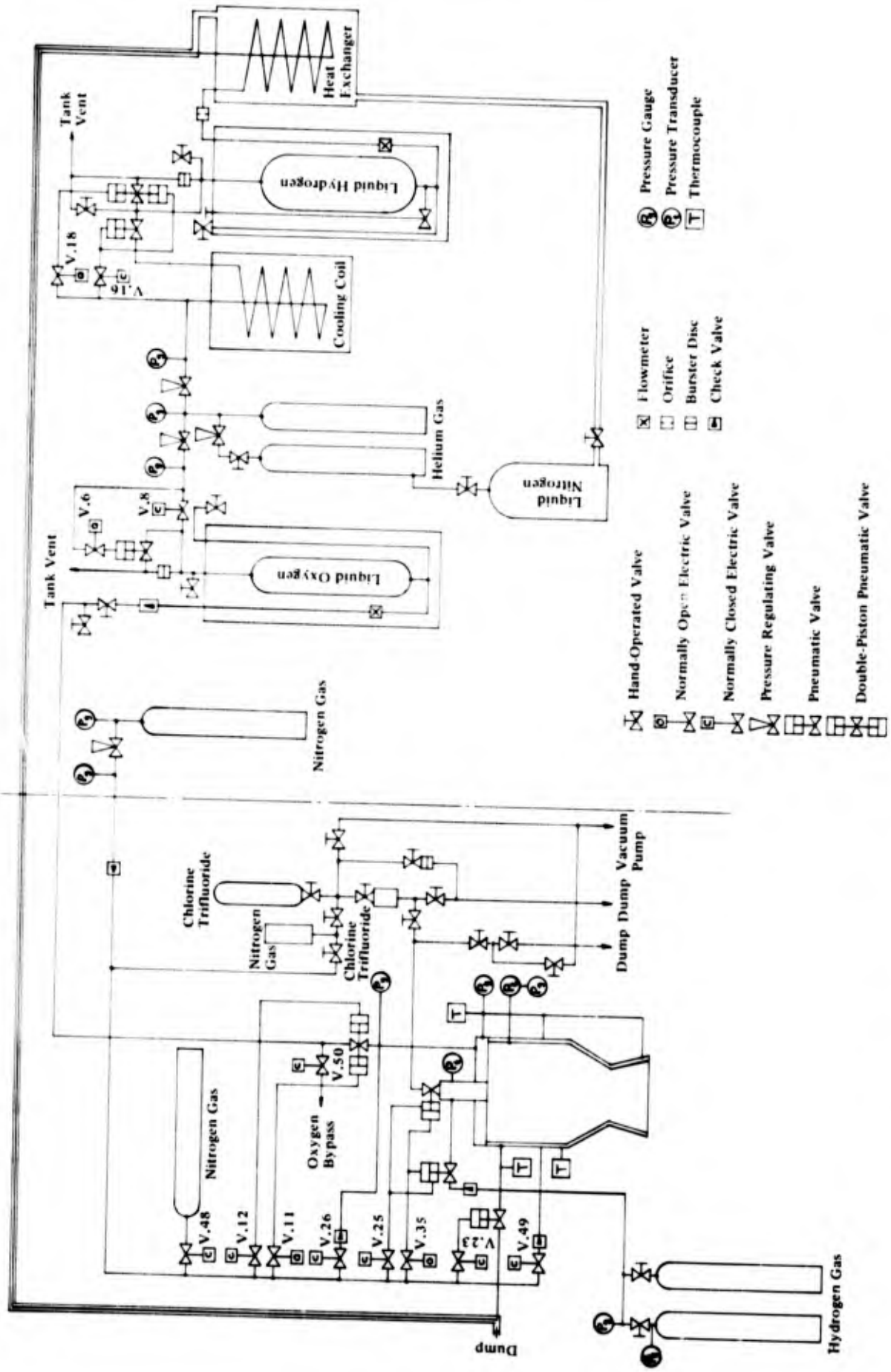

FIG. 10 : PROPELLANT FEED SYSTEM (SCHEMATIC) (PHASE II)

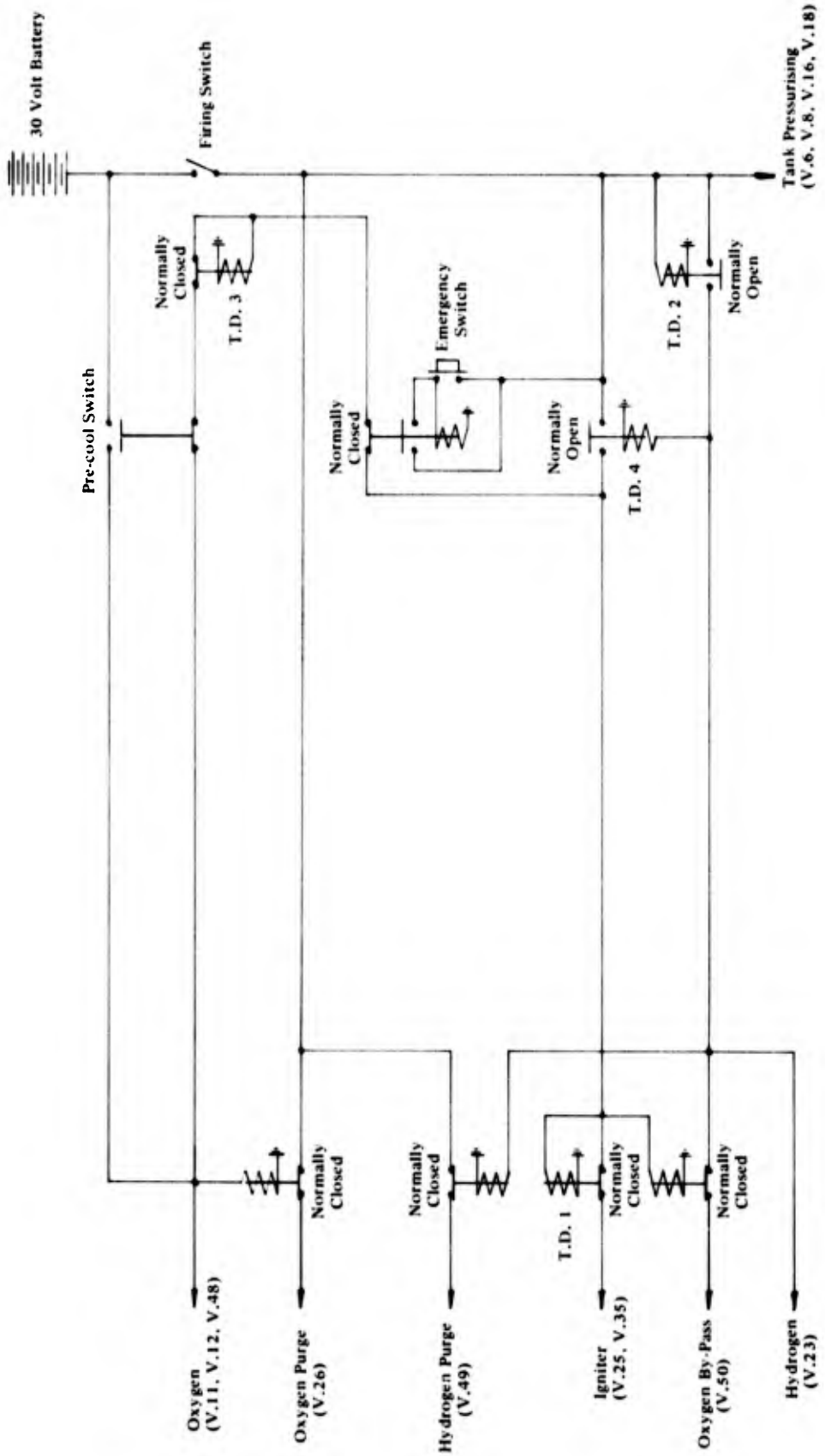

FIG. II : AUTOMATIC CONTROL CIRCUIT (SCHEMATIC) (PHASE II)

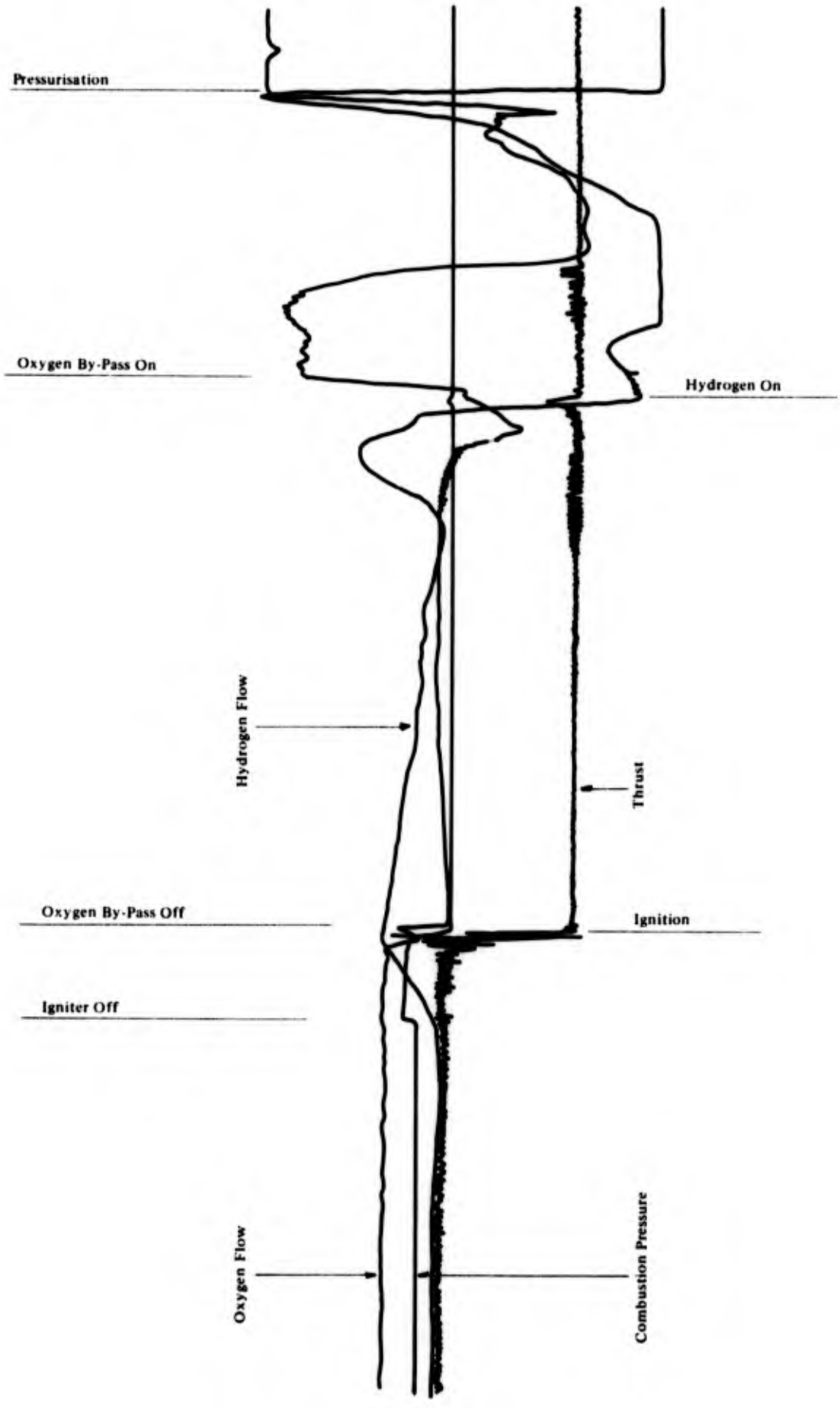

FIG. 12 : OSCILLOGRAPH RECORD OF EVENTS (FIRING NO. 5)

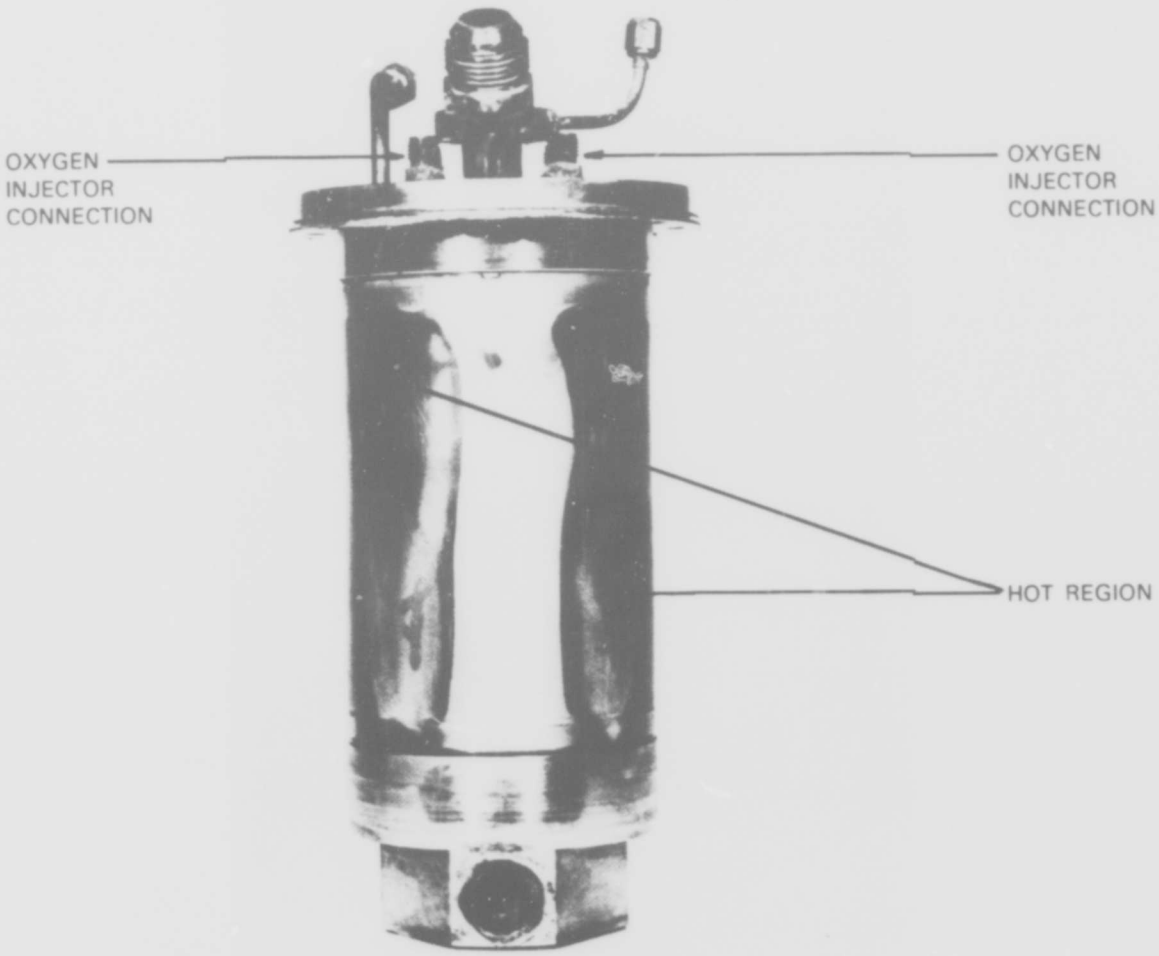

FIG. 13 : COMBUSTION CHAMBER LINER (PHASE II)